Observational Study

Medicine®

OPEN

Bicuspid aortic valve disease is associated with abnormal wall shear stress, viscous energy loss, and pressure drop within the ascending thoracic aorta

A cross-sectional study

Patrick Geeraert, BSc[a,b,c,d], Fatemehsadat Jamalidinan, PhD[a,b,c,d], Ali Fatehi Hassanabad, MD[a,b], Alireza Sojoudi, PhD[e], Michael Bristow, MD[a,f], Carmen Lydell, MD[a,g], Paul W.M. Fedak, MD, PhD[a], James A. White, MD[a,c], Julio Garcia, PhD[a,b,c,d,h,*]

Abstract

Bicuspid aortic valve (BAV) disease has significant gaps in its clinical management practices. To highlight the potential utility of advanced hemodynamic biomarkers in strengthening BAV assessment, we used 4-dimentional flow magnetic resonance imaging to investigate altered hemodynamics in the ascending aorta (AAo).

A total of 32 healthy controls and 53 age-matched BAV patients underwent cardiac magnetic resonance imaging at 3T, with cine imaging and 4D-flow. Analysis planes were placed along 3D-segmented aortas at the left ventricular outflow tract (LVOT), sinuses of Valsalva, mid-ascending aorta (MAA), and proximal to the first aortic branch. Locations were analyzed for aortic diameter (normalized to body surface area), pressure drop (PD), viscous energy loss (EL), and wall shear stress (WSS) sub-vectors (axial wall shear stress, circumferential wall shear stress [WSS_C], magnitude wall shear stress). Student's *t* tests, or non-parametric equivalents, compared parameters between cohorts. Univariable and multivariable analyses explored the associations of AAo diameter with hemodynamics within the BAV cohort.

Compared to control cohort, BAV patients showed significantly greater PD (MAA: 9.5 ± 8.0 vs 2.8 ± 2.4 mm Hg; $P < .01$), EL (from LVOT-AA1: 7.39 ± 4.57 mW vs 2.90 ± 1.07 mW; $P < .01$), and WSS_C (MAA: 0.3 ± 0.1 vs 0.2 ± 0.06 Pa; $P \leq .01$) throughout the AAo. Correlational analyses revealed an inverse association between AAo diameter and both magnitude wall shear stress and axial wall shear stress.

BAV patients exhibited increased PD, EL, and WSS_C in the AAo, and an inverse association between AAo diameter and WSS sub-vectors. This demonstrated the impact of PD, EL, and WSS in BAV disease and the importance of altered hemodynamics in aortic remodelling.

Abbreviations: 4D-flow MRI = 4-dimentional flow magnetic resonance imaging, AA1 = proximal to the first aortic branch, AAo = ascending aorta, BAV = bicuspid aortic valve, ECG = electrocardiogram, EL = viscous energy loss, EL_{index} = EL indexed to LVOT net flow, EL_{sys} = peak systolic EL, LV = left ventricle, LVOT = left ventricular outflow tract, MAA = mid-ascending aorta, MRA = magnetic resonance angiogram, MRI = magnetic resonance imaging, PC = phase-contrast, PD = pressure drop, PD_{sys} = peak systolic pressure drop, SOV = sinuses of Valsalva, WSS = wall shear stress, WSS_A = axial wall shear stress, WSS_C = circumferential wall shear stress, WSS_M = magnitude wall shear stress.

Keywords: 4D-flow MRI, aortic dilatation, bicuspid aortic valve, pressure drop, viscous energy loss, wall shear stress

Editor: Salvatore Patanè.

Julio Garcia received funding from the University of Calgary URGC SEM #1054341, and start-up funding from the Libin Cardiovascular Institute. Patrick Geeraert received minor funding for 2 summer studentships from Alberta Innovates. We acknowledge the support of the Conseil de recherche en science naturelles et en génie du Canada/Conseil de recherche en sciences naturelles et en genie du Canada RGPIN-2020–04549 and DGECR-2020-00204.

There are no conflicts of interest to disclose.

The datasets generated during and/or analyzed during the current study are available from the corresponding author on reasonable request.

[a] Department of Cardiac Sciences, [b] Department of Radiology, University of Calgary, Calgary, [c] Stephenson Cardiac Imaging Centre, University of Calgary, [d] Libin Cardiovascular Institute, [e] Circle Cardiovascular Imaging, Advanced Technologies, [f] Department of Medicine, [g] Diagnostic Imaging, University of Calgary, [h] Alberta Children's Hospital Research Institute, Calgary, AB, Canada.

[*] Correspondence: Julio Garcia, Department of Radiology and Cardiac Sciences, University of Calgary, SSB 0700, 1403 – 29 Street NW, Calgary, AB, T2N 2T9, Canada (e-mail: julio.garciaflores@ucalgary.ca).

How to cite this article: Geeraert P, Jamalidinan F, Hassanabad AF, Sojoudi A, Bristow M, Lydell C, Fedak PW, White JA, Garcia J. Bicuspid aortic valve disease is associated with abnormal wall shear stress, viscous energy loss, and pressure drop within the ascending thoracic aorta: A cross-sectional study. Medicine 2021;100:26(e26518).

Received: 3 October 2020 / Received in final form: 28 May 2021 / Accepted: 10 June 2021

http://dx.doi.org/10.1097/MD.0000000000026518

1. Introduction

Bicuspid aortic valve (BAV) disease is the most common congenital heart disease, affecting 1% to 2% of the general population.[1] These patients are recognized to be at increased risk of aortic aneurysm and/or dissection due to aortopathy.[2,3] However, definitive management strategies for BAV-associated aortopathy remain poorly defined. There is variability in current practice guidelines[4,5] while management strategies appear to vary substantially among cardiovascular surgeons.[6] Based upon these limitations significant emphasis has been placed on the investigation of alternative biomarkers for the description of BAV related aortopathy with the potential to improve risk prediction modelling in this patient population.

BAV disease has been recognized to alter ascending aorta (AAo) hemodynamics, catalyzing strong interest in non-invasive blood flow parameters that may demonstrate association with aortopathy disease progression. In particular, 4-dimensional (4D) flow magnetic resonance imaging (MRI) have presented unique opportunities to examine aortic hemodynamic parameters such as viscous energy loss (EL), pressure drop (PD), and wall shear stress (WSS). In the context of BAV disease, EL can provide estimates of permanent loss of kinetic energy experienced by blood via friction between adjacent fluid layers and may identify regions of excess energy transfer to aortic wall tissues and poor left-ventricular efficiency.[7] PD measurements can provide a previously validated[7–9] 3D representation of total pressure gradient drop along the aorta distal to the aortic valve.[10] Recognized limitations of cardiac catheterization and doppler echocardiography that lack consideration of downstream pressure recovery[11,12] can now be overcome by incorporating pressure recovery effects in 4D-flow-based evaluations.[13] Finally, WSS provides a representation of shear forces acting on the aortic wall as a result of friction with adjacent blood flow and has been implicated as a potential mediator of vessel wall remodeling using histopathology samples.[14] Of particular interest is the capacity to assess distinct sub-vectors of WSS[15] (Fig. 1), allowing delineation of axial WSS (parallel to vessel axis; axial wall shear stress [WSS_A]), circumferential WSS (around the circumference of the vessel; circumferential wall shear stress [WSS_C]), and net magnitude WSS (net sum of the previous 2 vectors; magnitude wall shear stress [WSS_M]), which offers potential discrimination of those vectors with greatest influence on vessel wall remodelling.

In this study, we applied 4-dimentional flow magnetic resonance imaging (4D-flow MRI) techniques to a cohort of patients with known BAV disease and healthy control subjects to

(i) identify associations between BAV disease and AAo EL, PD and WSS and
(ii) explore which of these hemodynamic parameters are most associated with objective markers of aortic remodelling.

We hypothesized that AAo EL, PD, and WSS would each be significantly altered in BAV patients and would demonstrate associations with AAo diameter measurements. Exploration of sub-vector components of WSS was also undertaken to identify which of these vectors may provide strongest association with markers of aortic remodelling.

2. Methods

2.1. Study population

A total of 85 subjects were prospectively recruited; 53 BAV patients who were clinically referred for an MRI scan and 32 healthy controls who were recruited for research purposes. The BAV patients (19 female) were 44 ± 16 years old, consisting of 14 Type 0 phenotype, 35 Type 1 phenotype, 3 Type 2 phenotype, and 1 unidentified phenotype. The mean age of the healthy controls (10 female) was 41 ± 15 years old. Patients were recruited under an a-priori sub-study of the Cardiovascular Imaging Registry of Calgary (REB13-0902), a prospective observational registry at the Libin Cardiovascular Institute, University of Calgary. The study was coordinated using Acuity (Cohesic Inc., Calgary, Alberta) for the delivery of patient informed consent, health questionnaires and for collection of standard MRI-related variables.

Patients were required to be $\geq$18 years of age with not more than mild mitral valve insufficiency. Patients with any evidence of significant systolic dysfunction (left ventricle ejection fraction $<$ 50%), history of known ischemic or non-ischemic cardiomyopathy, or complex congenital heart disease were excluded, as were patients with implantable devices or other recognized contra-indications to MRI. Healthy control subjects were required to be

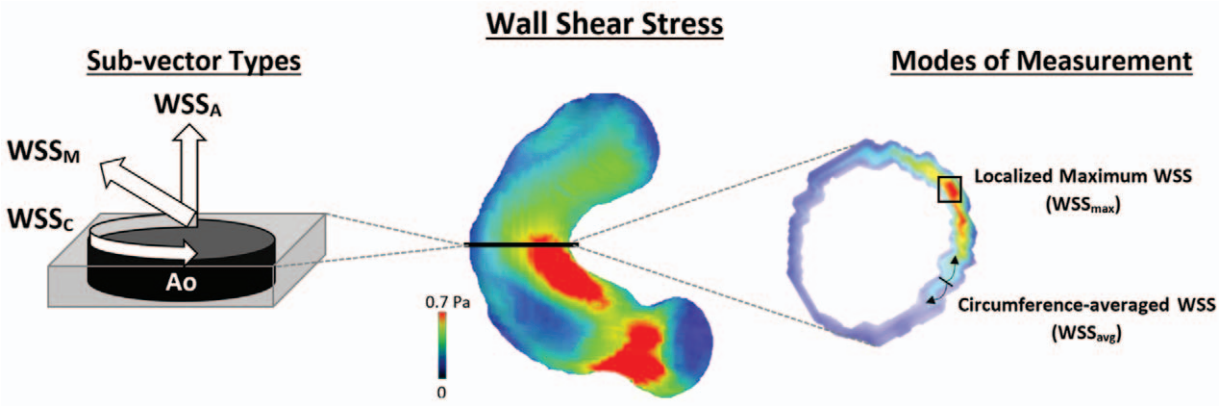

Figure 1. The illustrated definitions of (i) axial, circumferential, and magnitude WSS sub-vectors (left) and (ii) the 2 methods of measuring these WSS sub-vectors at aortic locations. Ao, aorta; BAV, bicuspid aortic valve; WSS, wall shear stress; WSS_A, axial wall shear stress; WSS_C, circumferential wall shear stress; WSS_M, magnitude wall shear stress; WSS_{avg}, circumference-averaged WSS; WSS_{max}, localized maximum WSS.

≥18 years of age and have no history of cardiovascular disease, diabetes, or uncontrolled hypertension. Blood pressure was excluded from demographic analyses, as it was not retrospectively available for certain subjects.

The study was approved by the Conjoint Health Research Ethics Board at the University of Calgary and all subjects provided written informed consent. All research activities were performed in accordance with the Declaration of Helsinki.

2.2. Cardiac magnetic resonance imaging protocol

MRI examinations were performed using 3T MRI scanners (Skyra [n = 17], Prisma [n = 70], Siemens, Erlangen, Germany). All patients underwent a standardized imaging protocol inclusive of retrospectively electrocardiogram-gated, time-resolved balanced steady-state free precession cine imaging in 4-chamber, 3-chamber, 2-chamber, and short-axis views of the left ventricle (LV) at end-expiration. A contrast-enhanced 3D magnetic resonance angiogram (MRA) of the thoracic aorta was performed in all subjects for assessing aortic structure in accordance with local clinical protocols using administration of 0.1 mmol/kg gadolinium contrast (Gadovist, Bayer, Canada). Approximately 5 to 10 minutes following contrast administration a retrospectively electrocardiogram-gated, time-resolved 3D phase-contrast (PC) MRI with 3-directional velocity encoding (4D-flow MRI, Siemens WIP 785A) was performed to measure in vivo 3D blood flow velocities for the whole heart. 4D-flow MRI data were acquired during free breathing using navigator gating of diaphragmatic motion.[16] 4D-flow MRI pulse sequence parameters were as follows: flip angle = 15°; spatial resolution = 2.0–3.6 mm × 2.0–3.0 mm × 2.5–3.5 mm; temporal resolution = 25–35 ms; velocity sensitivity = 150–200 cm/second. Total acquisition time was typically between 7 and 15 minutes, depending on heart rate and respiratory navigator efficiency. The number of phases varied with clinical scan operator from 25 to 30.

2.3. 4D-flow MRI analysis

A workflow diagram is provided in Figure 2. All analyses were completed by a single observer using cvi[42] version 5.11.5 (Circle Cardiovascular Imaging Inc., Calgary, Canada). All subjects' 4D-flow MRI data underwent preprocessing to execute corrections for Maxwell terms, eddy current-induced phase offset, static tissue, and velocity aliasing, when necessary.[16] An entire cardiac 3D PC MRA was generated for each subject using the preprocessed 4D-flow MRI data, as previously described.[16–18] This 3D PC MRA was used to perform a 3D segmentation of the thoracic aorta, inclusive of the left ventricular outflow tract (LVOT). In accordance with standard procedures,[19] analysis planes were placed at 4 distinct locations of the thoracic aorta segmentation: LVOT, sinuses of Valsalva (SOV), mid-ascending aorta (MAA), and proximal to the first aortic arch branch (AA1).

Several standard flow parameters were calculated at each of the 4 analysis planes: peak systolic blood velocity, net flow, and regurgitation fraction.[20,21] For the purposes of this study, "peak systolic" values are defined as the largest measurement value within 3 phases before/after peak systole phase (normally phase 4–7).

The 3D time-resolved velocity fields provided by 4D-flow MRI allowed for the calculation of 3 advanced flow parameters: EL, PD, and WSS. EL estimates the instantaneous viscous dissipation rate (mW) on a voxel-by-voxel basis[22] and was analyzed within the total vessel volume from LVOT to AA1 (Fig. 2), rather than at each individual analysis plane. We report 2 measures of EL:

(i) peak systolic EL at any point within the entire LVOT-AA1 volume (peak systolic EL [EL_{sys}]; mW), and
(ii) this same value indexed to LVOT net flow (EL indexed to LVOT net flow [EL_{index}]; mW/mL).

PD measurements have demonstrated clinical feasibility[9] and are calculated by a previously validated extended Bernoulli equation – which demonstrates accurate inclusion of the pressure recovery phenomenon.[9,10] PD was analyzed at each analysis plane and reported as a peak systolic deviance to the pressure value at LVOT (peak systolic pressure drop [PD_{sys}]; mm Hg).

WSS measurements estimate the shear forces present on the aortic wall due to friction with adjacent blood flow. Three sub-vectors, WSS_A, and WSS_C, WSS_M, were computed via methods validated by Stalder et al[15] and represent, respectively, WSS

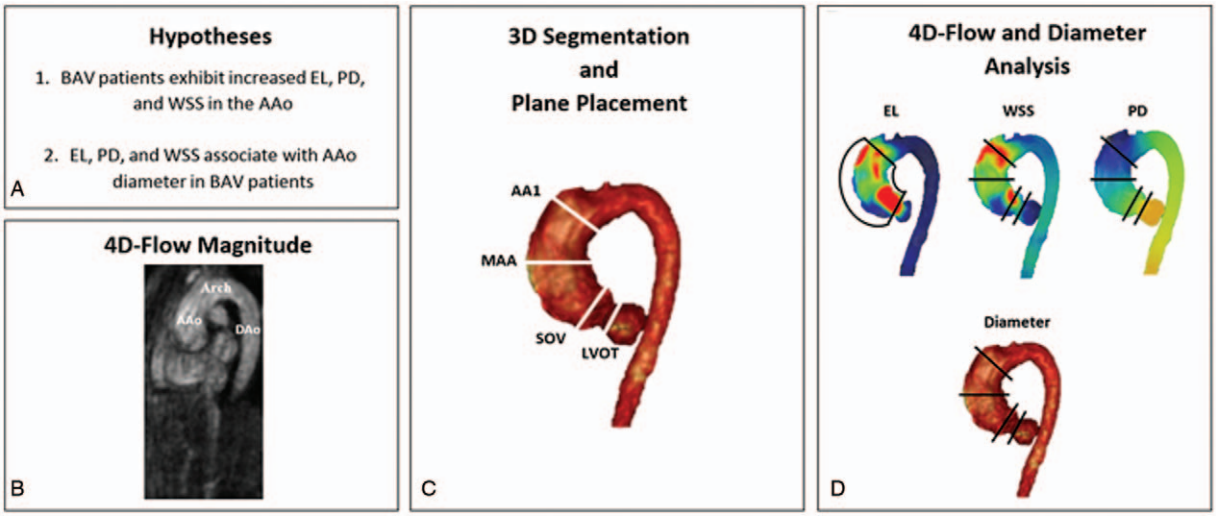

Figure 2. Workflow diagram of study methods. AAo, ascending aorta; AA1, proximal to first aortic branch; BAV, bicuspid aortic valve; DAo, descending aorta; EL, viscous energy loss; LVOT, left ventricular outflow tract; MAA, mid-ascending aorta; PD, pressure drop; SOV, sinuses of Valsalva; WSS, wall shear stress.

forces acting parallel to the vessel, around the inner circumference of the vessel wall, and in the overall net magnitude direction (Fig. 1). Illustrated by Figure 1, each of these 3 sub-vectors are reported as 2 distinct measures:

(i) the peak systolic value at a localized region of the vessel wall (peak systolic WSS $[WSS_x]_{,max}$; x denotes the subscript A, C, or M) and
(ii) the peak systolic value averaged over the circumference of the vessel wall.

2.4. Aortic vessel diameters

Maximum aortic diameters were calculated at each analysis plane using 3D PC MRA in accordance with standard procedures.[19] Raw diameter values were also indexed to body surface area (mm/m^3), as this has been shown to provide better risk stratification for aortic aneurysms.[23] For this study, if a patient exhibited a SOV and/or MAA diameter exceeding 40 mm then they were classified as having AAo dilation.

2.5. Statistical analysis

Four a-priori analyses were performed. The first, and primary, compared all BAV patients (n = 53) to healthy volunteers (n = 32). The second compared Type 0 BAV (n = 14) to Type 1 BAV (n = 35); Type 2 BAV cohort (n = 3) was too small for adequate statistical analyses. The third compared patients with a dilated AAo (SOV and/or MAA > 40 mm) to those exhibiting no dilation (<40 mm). The 4 compared matched peak velocity and regurgitant fraction controls with no dilation BAV (n = 11). The fifth analysis compared males (n = 56) to females (n = 29) for exploratory purposes. BAV valve phenotypes were evaluated via 2-dimentional cine valve acquisitions and categorized according to Sievers' classifications.[24]

Histograms were evaluated and Shapiro–Wilks normality tests were conducted to determine the distribution of parameters in each cohort separately and all cohorts collectively. A chi-square test was used to evaluate differences in sex proportions between BAV patients and controls and between BAV valve phenotypes. Using the student's t test, or non-parametric equivalent, each cohort pair was analyzed for differences in parameters. Within the BAV cohort only, indexed aortic diameters were correlated with demographic and flow parameters to obtain Pearson or Spearman correlation coefficients. Additionally, multiple linear regression was performed to determine independent association of 4D-flow parameters with aortic vessel diameters within the BAV cohort. Instead of stratifying data points by their respective aortic region (each region having n = 53 data points), the multiple linear regression model assessed all data points in the SOV, MAA, and AA1 collectively (a total of n = 159 data points), using indexed diameter as the dependent variable and age, EL_{index}, PD_{sys}, $WSS_{M,avg}$, and $WSS_{A,avg}$ as the independent variables. Before performing multiple linear regression, all correlates were checked for linearity, multivariate normality, homoscedasticity, and the absence of collinearity.

For all statistical tests, a P-value of less than .05 was considered significant. In addition, bivariate correlations were only considered significant of the correlation coefficient was greater than absolute 0.3. All statistics were performed in SPSS 25 (Chicago, IL).

3. Results

3.1. Study population

Baseline demographics of the study population are provided in Table 1. BAV patients and healthy controls were age matched ($P = .9$). The respective prevalence of Type 0, Type 1, and Type 2 BAV phenotypes were 26%, 66%, and 6%. Twenty-five (47%) patients were classified as non-dilated, while 28 (53%) met AAo dilation criteria. Fifteen BAV patients (28%) had mild transvalvular velocity and 7 (13%) had moderate peak velocity. Most BAV patients had minimal aortic regurgitation fraction (<30%), and 4 cases had moderate regurgitation fraction (between 30% and 50%). Due to low power, the Type 2 BAV phenotype cohort was excluded from BAV phenotype-specific statistical analyses. Blood pressure and stenosis measures were excluded due to incomplete data.

3.2. Aortic remodelling and general flow characteristics

BAV patients demonstrated significantly greater indexed aortic diameters than healthy controls throughout the AAo (e.g,. MAA: $19 \pm 4\,mm/m^2$ vs $15 \pm 2\,mm/m^2$; $P < .01$) as shown in Table 2. In contrast to controls, BAV patients demonstrated significantly greater peak systolic blood velocity at all AAo regions (e.g., MAA: 155 ± 53 cm/s vs 113 ± 25 cm/s; $P < .01$). BAV subjects also showed a greater regurgitant fraction at all AAo locations (e.g., MAA: $20 \pm 21\%$ vs $3 \pm 3\%$; $P < .01$) as well as lower net forward flow at the MAA (63 ± 22 mL vs 75 ± 19 mL; $P < .01$).

Table 1

Cohort demographics.

	Cohort										
Variable	**Control**	**BAV**	***P***	**Type 0**	**Type 1**	***P***	**Male**	**Female**	***P***	**Non-dilated BAV**	**Dilated BAV**	***P***
Count (n)	31	53	–	14	35	–	55	29	–	25	28	–
Female (n)	10	19	.4	5	13	.9	–	–	–	10	9	.6
Age (yrs)	41 ± 15	44 ± 16	.9	44 ± 13	45 ± 17	.8	44 ± 15	41 ± 17	.4	40 ± 17	47 ± 15	.06
BSA (m^2)	1.9 ± 0.3	2.0 ± 0.3	.07	2.0 ± 0.2	2.0 ± 0.3	.9	2.1 ± 0.2	1.8 ± 0.2	<.01	1.9 ± 0.3	2.0 ± 0.2	.9
LVEF (%)	61 ± 4	61 ± 7	.8	63 ± 7	61 ± 6	.5	60 ± 6	63 ± 5	.1	59 ± 5	62 ± 8	.4
LVESV (mL)	61 ± 18	77 ± 33	.06	66 ± 36	73 ± 27	.6	79 ± 33	57 ± 14	<.01	77 ± 29	76 ± 37	.9
LVEDV (mL)	165 ± 33	191 ± 61	.04	170 ± 62	186 ± 55	.5	199 ± 58	154 ± 33	<.01	189 ± 65	191 ± 60	.9
LV mass (g)	107 ± 30	119 ± 39	.2	108 ± 22	119 ± 41	.5	124 ± 36	99 ± 30	.01	117 ± 37	121 ± 41	.7

Student's t test used for parametric variables; non-parametric equivalent used for non-parametric variables. BAV, bicuspid aortic valve; BSA, body surface area; LV, left ventricle; LVEF, left ventricle ejection fraction; *P*, *P*-value; Type 0, Sievers's type 0 BAV; Type 1, Sievers's type 1 BAV.

Table 2

Contrasts between control and BAV cohorts at each analysis location.

	Location											
	LVOT			SOV			MAA			AA1		
Parameter	Control	BAV	*P*	Control	BAV	*P*	Control	BAV	*P*	Control	BAV	*P*
Indexed diameter (mm/m^2)	13.23 ± 1.73	14.44 ± 2.00	<.01	14.21 ± 2.32	19.40 ± 3.60	<.01	14.81 ± 2.17	19.04 ± 4.05	<.01	13.86 ± 2.18	15.62 ± 3.63	.02
Net flow (mL)	79.41 ± 19.10	84.28 ± 19.58	.3	87.00 ± 20.96	77.98 ± 19.67	.05	74.50 ± 19.36	62.61 ± 22.00	.02	72.85 ± 18.06	64.29 ± 2130	.06
Regurgitation (%)	2.04 ± 2.22	9.02 ± 11.25	<.01	1.42 ± 1.72	12.58 ± 13.94	<.01	2.67 ± 3.19	19.90 ± 21.13	<.01	2.61 ± 4.21	18.28 ± 17.61	<.01
Peak velocity (m/s)	1.16 ± 0.18	1.10 ± 0.22	.6	1.44 ± 0.16	2.05 ± 0.65	<.01	1.13 ± 0.25	1.55 ± 0.53	<.01	0.98 ± 0.25	1.24 ± 0.38	<.01
$WSS_{M,avg}$ (Pa)	0.17 ± 0.06	0.12 ± 0.06	<.01	0.18 ± 0.07	0.12 ± 0.07	<.01	0.19 ± 0.07	0.15 ± 0.07	.2	0.22 ± 0.07	0.20 ± 0.08	.2
$WSS_{M,max}$ (Pa)	0.73 ± 0.18	0.74 ± 0.21	.8	0.84 ± 0.26	0.93 ± 0.27	.2	0.76 ± 0.24	1.00 ± 0.29	.04	0.73 ± 0.20	0.88 ± 0.29	.1
$WSS_{A,avg}$ (Pa)	0.48 ± 0.13	0.45 ± 0.13	.3	0.36 ± 0.17	0.23 ± 0.13	<.01	0.37 ± 0.12	0.37 ± 0.13	1.0	0.43 ± 0.10	0.45 ± 0.14	.5
$WSS_{A,max}$ (Pa)	0.65 ± 0.15	0.60 ± 0.17	.4	0.66 ± 0.21	0.67 ± 0.23	.9	0.56 ± 0.18	0.71 ± 0.25	.01	0.62 ± 0.24	0.65 ± 0.22	.6
$WSS_{C,avg}$ (Pa)	0.10 ± 0.03	0.12 ± 0.04	<.01	0.10 ± 0.02	0.13 ± 0.05	<.01	0.15 ± 0.06	0.27 ± 0.11	<.01	0.11 ± 0.06	0.24 ± 0.14	<.01
$WSS_{C,max}$ (Pa)	0.25 ± 0.14	0.27 ± 0.12	.6	0.31 ± 0.13	0.38 ± 0.17	.2	0.32 ± 0.12	0.46 ± 0.21	<.01	0.27 ± 0.11	0.35 ± 0.18	.2
PD_{sys} (mm Hg)	–	–	–	1.16 ± 1.43	5.42 ± 4.47	<.01	2.80 ± 2.37	9.48 ± 7.95	<.01	3.23 ± 2.59	8.39 ± 9.23	<.01

LVOT, left ventricular outflow tract; MAA, mid-ascending aorta; PD, pressure drop.

No differences in general flow characteristics were seen between non-dilated and dilated patients. No significant differences in values were found between Type 1 and Type 0 valve cohorts.

Sex-based analyses demonstrated that male subjects had significantly greater net forward flow at the LVOT (88 ± 20 mL vs 72 ± 13 mL; $P < .01$), SOV (86 ± 22 mL vs 72 ± 14 mL; $P < .01$), and AA1 (71 ± 20 mL vs 60 ± 19 mL; $P = .01$). Upon normalizing for body surface area, these differences in net forward flow disappear.

3.3. Wall shear stress, pressure drop, and viscous energy loss

Compared to controls, BAV patients demonstrated significantly lower $WSS_{M,avg}$ (0.12 ± 0.07 Pa vs 0.18 ± 0.07 Pa; $P < .01$) and $WSS_{A,avg}$ (0.23 ± 0.1 Pa vs 0.36 ± 0.2 Pa; $P < .01$) at the SOV, as shown in Table 2 and Figure 3. However, $WSS_{C,avg}$ was significantly higher at all locations (e.g., MAA: 0.27 ± 0.1 Pa vs 0.15 ± 0.06 Pa; $P < .01$). When analyzing localized maximum WSS values BAV patients exhibited significantly greater $WSS_{M,max}$ (1.00 ± 0.28 Pa vs 0.76 ± 0.24 Pa; $P = .04$), $WSS_{A,max}$ (0.71 ± 0.25 Pa vs 0.56 ± 0.18 Pa; $P = .01$), and $WSS_{C,max}$ (0.46 ± 0.21 Pa vs 0.32 ± 0.12 Pa; $P < .01$) at the MAA. Example cases are illustrated in Figure 4. PD_{sys} was significantly greater in BAV than controls throughout the entire AAo (e.g., MAA: 9.48 ± 7.95 mm Hg vs 2.80 ± 2.37 mm Hg; $P < .01$), shown in Table 2 and Figure 3. BAV patients also demonstrated greater aortic EL_{sys} (7.39 ± 4.57 mW vs 2.90 ± 1.07 mW; $P < .01$) and EL_{index} (0.090 ± 0.052 mW/mL vs 0.037 ± 0.011 mW/mL; $P < .01$) than controls (Fig. 3).

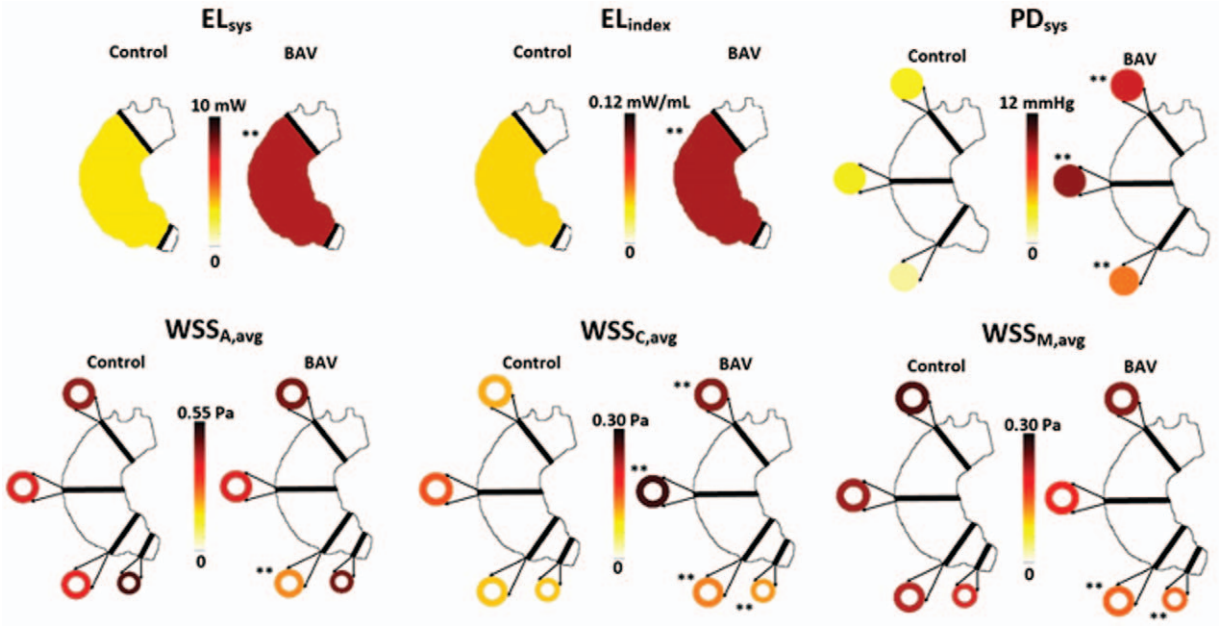

Figure 3. Hemodynamic contrasts between controls and BAV cohorts. Each color-coded value represents the mean value of its respective cohort. BAV, bicuspid aortic valve; EL_{index}, peak systolic viscous energy loss normalized to LVOT net flow; EL_{sys}, peak systolic viscous energy loss; LVOT, left ventricular outflow tract; PD_{sys}, peak systolic pressure drop; $WSS_{A,avg}$, circumference-averaged axial wall shear stress; $WSS_{C,avg}$, circumference-averaged circumferential wall shear stress; $WSS_{M,avg}$, circumference-averaged magnitude wall shear stress. $^{**}P < 0.01$.

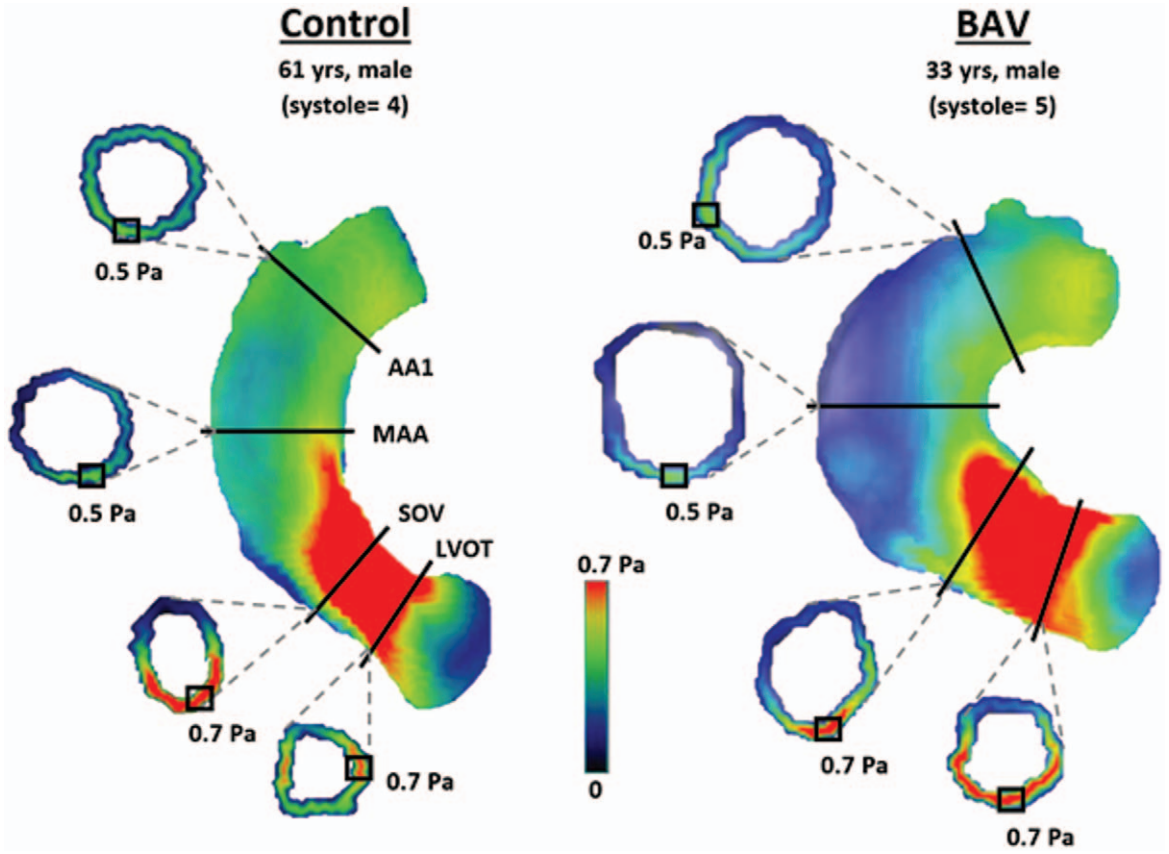

Figure 4. Visualized examples of localized maximum WSS_M values at each aortic location in a healthy control and a BAV patient. AA1, proximal to first aortic branch; BAV, bicuspid aortic valve; LVOT, left ventricular outflow tract; MAA, mid-ascending aorta; SOV, sinuses of Valsalva; WSS, wall shear stress; WSS_M, magnitude wall shear stress; yrs, years old.

Compared to non-dilated patients, patients with AAo dilation exhibited reduced $WSS_{M,avg}$ at the LVOT (0.14 ± 0.06 vs 0.11 ± 0.06 Pa; $P = .02$), MAA (0.19 ± 0.06 vs 0.11 ± 0.05 Pa; $P < .01$), and AA1 (0.23 ± 0.09 vs 0.17 ± 0.08 Pa; $P = .01$), and reduced $WSS_{A,avg}$ at the LVOT (0.49 ± 0.14 vs 0.42 ± 0.11 Pa; $P = .04$) and AA1 (0.49 ± 0.16 vs 0.41 ± 0.12 Pa; $P = .04$), as shown in Table 3. In terms of localized maximum WSS, dilated patients had reduced $WSS_{M,max}$ values at the SOV only (1.03 ± 0.26 vs 0.84 ± 0.25 Pa; $P < .01$). No other parameters differed significantly between dilation cohorts.

Matched cases of controls and no dilated BAV (n = 11) had similar peak velocity (111 ± 18 cm/s vs 110 ± 19 cm/s, $P = .827$),

Table 3

Contrasts between BAV patients with and without aortic dilation.

	Location											
	LVOT			SOV			MAA			AA1		
Parameter	Non-dilated	Dilated	*P*	Non-dilated	Dilated	*P*	Non-dilated	Dilated	*P*	Non-dilated	Dilated	*P*
Regurgitation (%)	7.84 ± 11.62	10.29 ± 11.38	.7	9.83 ± 10.53	15.40 ± 16.28	.9	14.48 ± 14.64	25.40 ± 24.78	.7	14.09 ± 14.98	21.57 ± 19.69	.1
Peak velocity (m/s)	1.14 ± 0.22	1.07 ± 0.23	.3	1.97 ± 0.59	2.11 ± 0.72	.7	1.45 ± 0.35	1.62 ± 0.64	.2	1.22 ± 0.35	1.24 ± 0.43	.8
$WSS_{M,avg}$ (Pa)	0.14 ± 0.06	0.11 ± 0.06	.02	0.15 ± 0.09	0.10 ± 0.05	.1	0.19 ± 0.06	0.11 ± 0.05	<.01	0.23 ± 0.09	0.17 ± 0.08	.01
$WSS_{M,max}$ (Pa)	0.78 ± 0.23	0.71 ± 0.19	.3	1.03 ± 0.26	0.84 ± 0.25	<.01	1.01 ± 0.28	0.98 ± 0.29	.9	0.93 ± 0.27	0.83 ± 0.31	.2
$WSS_{A,avg}$ (Pa)	0.49 ± 0.14	0.42 ± 0.11	.04	0.30 ± 0.15	0.17 ± 0.09	.07	0.40 ± 0.12	0.33 ± 0.13	.07	0.49 ± 0.16	0.41 ± 0.12	.04
$WSS_{A,max}$ (Pa)	0.60 ± 0.17	0.60 ± 0.16	.9	0.72 ± 0.24	0.63 ± 0.21	.2	0.74 ± 0.23	0.68 ± 0.27	.8	0.69 ± 0.18	0.61 ± 0.25	.07
$WSS_{C,avg}$ (Pa)	0.12 ± 0.03	0.13 ± 0.04	.3	0.14 ± 0.06	0.13 ± 0.04	.9	0.25 ± 0.10	0.28 ± 0.13	.3	0.26 ± 0.16	0.23 ± 0.12	.9
$WSS_{C,max}$ (Pa)	0.26 ± 0.12	0.27 ± 0.12	.9	0.35 ± 0.16	0.40 ± 0.18	.3	0.45 ± 0.22	0.47 ± 0.21	.6	0.33 ± 0.16	0.35 ± 0.21	.6
PD_{sys} (mm Hg)	–	–	–	5.47 ± 4.54	5.40 ± 4.64	.7	9.56 ± 7.75	9.40 ± 8.53	.7	9.00 ± 9.15	8.02 ± 9.71	.9

Student's *t* test used for parametric variables; non-parametric equivalent used for non-parametric variables. PD_{sys} is reported as a difference from LVOT pressure at peak systole. AA1, proximal to first aortic branch; BAV, bicuspid aortic valve; LVOT, left ventricular outflow tract; MAA, mid-ascending aorta; *P*, *P*-value; PD, pressure drop; PD_{sys}, pressure drop; SOV, sinuses of Valsalva; $WSS_{A,avg}$, circumference-averaged peak systolic axial wall shear stress; $WSS_{A,max}$, localized peak systolic axial wall shear stress; $WSS_{C,avg}$, circumference-averaged peak systolic circumferential wall shear stress; $WSS_{C,max}$, localized peak systolic circumferential wall shear stress; $WSS_{M,avg}$, circumference-averaged peak systolic net magnitude wall shear stress; $WSS_{M,max}$, localized peak systolic net magnitude wall shear stress.

Table 4

Correlations between indexed diameter and variables of interest at separate regions and all regions collectively.

Correlates	Location							
Indexed diameter vs:	SOV		MAA		AA1		Collective	
	R	*P*	*R*	*P*	*R*	*P*	*R*	*P*
Age	0.065	.7	0.23	.1	0.32	.02	0.09	.2
EL_{index}	0.04	.8	0.31	.03	0.30	.03	0.09	.2
$WSS_{M,avg}$	−0.43	<.01	−0.53	<.01	−0.42	<.01	−0.32	<.01
$WSS_{M,max}$	−0.54	<.01	−0.05	.7	−0.10	.5	0.02	.8
$WSS_{A,avg}$	−0.34	<.01	−0.22	.1	−0.50	<.01	−0.51	<.01
$WSS_{A,max}$	−0.40	<.01	−0.15	.3	−0.14	.3	−0.07	.3
$WSS_{C,avg}$	0.10	.5	0.26	.1	0.06	.7	0.09	.2
$WSS_{C,max}$	0.07	.6	0.08	.6	0.12	.4	0.23	<.01
PD_{sys}	−0.43	<.01	0.14	.3	0.06	.7	−0.10	.3

Analysis pertains to BAV cohort only. Pearson correlation used when both variables were parametric, Spearman's correlation used when at least 1 variable was non-parametric. AA1, proximal to first aortic branch; BAV, bicuspid aortic valve; EL_{index}, peak systolic viscous energy loss normalized to net flow; MAA, mid-ascending aorta; *P*, *P*-value; PD, pressure drop; PD_{sys}, peak systolic pressure drop; *R*, correlation coefficient; SOV, sinuses of Valsalva; $WSS_{A,avg}$, circumference-averaged peak systolic axial wall shear stress, $WSS_{A,max}$, localized peak systolic axial wall shear stress, $WSS_{C,avg}$, circumference-averaged peak systolic circumferential wall shear stress; $WSS_{C,max}$, localized peak systolic circumferential wall shear stress; $WSS_{M,avg}$, circumference-averaged peak systolic net magnitude wall shear stress; $WSS_{M,max}$, localized peak systolic net magnitude wall shear stress.

and similar regurgitation fraction (2 ± 2% vs 3 ± 2%, *P* = .315). SOV PD_{sys} was higher in BAV than controls (4.31 ± 3.19 mm Hg vs 1.00 ± 1.64 mm Hg, *P* = .006). At mid ascending aorta was slightly elevated in BAV for $WSS_{M,max}$ (0.90 ± 0.13 Pa vs 0.69 ± 0.25 Pa, *P* = .02), $WSS_{A,max}$ (0.65 ± 0.13 Pa vs 0.49 ± 0.17 Pa, *P* = .02), $WSS_{C,avg}$ (0.20 ± 0.05 Pa vs 0.15 ± 0.05 Pa, *P* = .03), and PD_{sys} (8.57 ± 6.53 mm Hg vs 3.25 ± 2.48 mm Hg, *P* = .02). Similarly, at aortic arch for $WSS_{M,max}$ (0.85 ± 0.21 Pa vs 0.65 ± 0.16 Pa, *P* = .023) and $WSS_{C,avg}$ (0.20 ± 0.08 Pa vs 0.09 ± 0.06 Pa, *P* = .002).

Type 1 versus Type 0 valve groups differed significantly for $WSS_{M,avg}$ at the LVOT (0.13 ± 0.065 Pa vs 0.10 ± 0.033 Pa, respectively; *P* = .01), $WSS_{C,avg}$ at the AA1 (0.22 ± 0.15 Pa vs 0.30 ± 0.10 Pa; *P* = .03), $WSS_{C,max}$ at the MAA and AA1 (e.g., MAA: 0.41 ± 0.17 Pa vs 0.56 ± 0.22 Pa; *P* = .048), and PD_{sys} at the MAA (8.69 ± 7.31 mm Hg vs 8.87 ± 3.54 mm Hg; *P* = .02).

Sex-based analyses demonstrated that males and females only differed significantly in $WSS_{C,max}$ when assessed at the SOV (0.38 ± 0.17 Pa vs 0.32 ± 0.13 Pa, respectively; *P* = .02). No other parameters showed any significant differences between sexes.

3.4. Associations with aortic remodelling – univariable analyses

Univariable analysis results are shown in Table 4 and Figures 5 and 6. Age was associated with increased aortic diameters within the BAV cohort at AA1 location only (*R* = 0.32, *P* = .02). EL_{index} was associated with increased aortic dimensions at the MAA (*R* = 0.31, *P* = .03) and AA1 (*R* = 0.30, *P* = .03). PD_{sys} was inversely correlated with indexed diameter at the SOV only (*R* = −0.43, *P* < .01).

$WSS_{M,avg}$ was negatively associated with indexed diameter throughout the entire AAo (e.g., MAA: *R* = −0.53, *P* < .01) while $WSS_{A,avg}$ was negatively associated at the SOV and AA1 only (*R* = −0.34, *P* = .01 and *R* = −0.50, *P* < .01, respectively). In

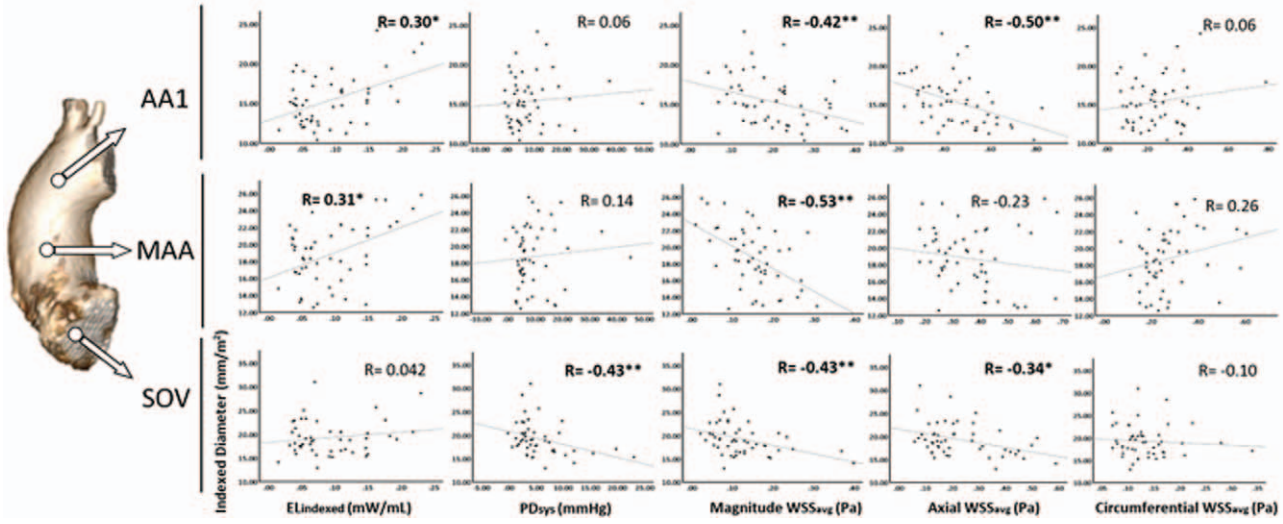

Figure 5. Correlations between indexed diameter and several 4D-Flow parameters at each aortic location separately. AA1, proximal to first aortic branch; EL_{index}, peak systolic viscous energy loss indexed to left ventricular outflow tract net flow; MAA, mid-ascending aorta; PD_{sys}, peak systolic pressure drop; *R*, correlation coefficient; SOV, sinuses of Valsalva; WSS_{avg}, circumference-averaged wall shear stress. $^{*}P < 0.05$, $^{**}P < 0.01$.

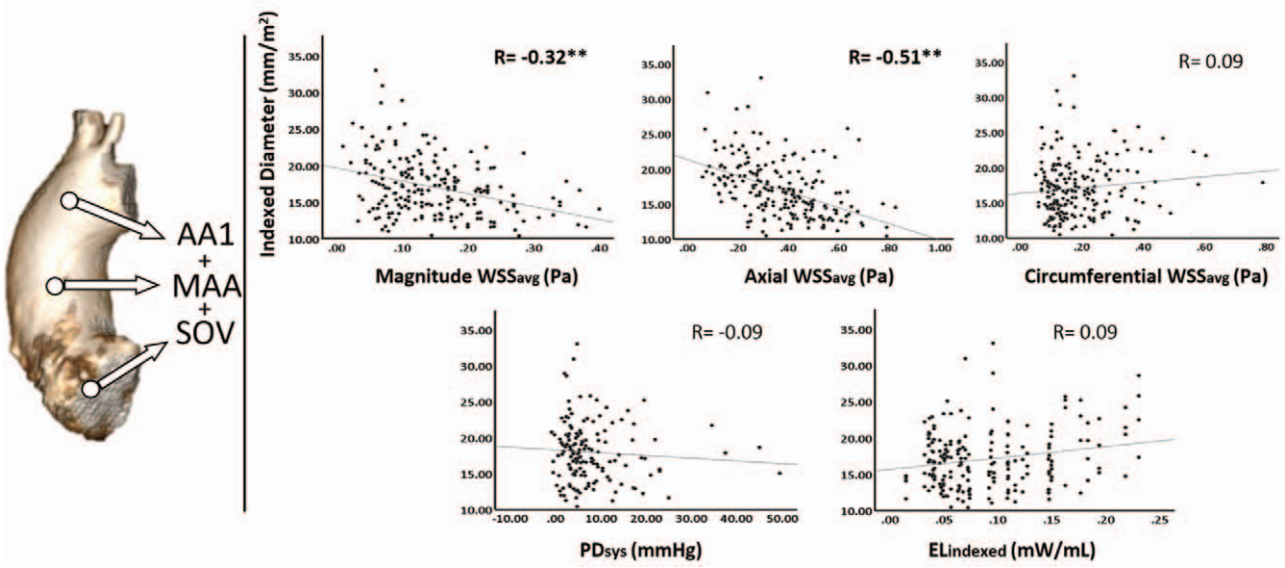

Figure 6. Correlations between indexed diameter and several 4D-Flow parameters at all aortic locations collectively. AA1, proximal to first aortic branch; EL_{index}, peak systolic viscous energy loss indexed to left ventricular outflow tract net flow; MAA, mid-ascending aorta; PD_{sys}, peak systolic pressure drop; *R*, correlation coefficient; SOV, sinuses of Valsalva; WSS_{avg}, circumference-averaged wall shear stress. $^{*}P<0.05$, $^{**}P<0.01$.

contrast to the circumference-averaged WSS values, $WSS_{M,max}$ and $WSS_{A,max}$ correlated negatively with indexed diameter at the SOV only ($R=-0.54$, $P<.01$ and $R=-0.40$, $P<.01$, respectively). Considering all aortic locations together from LVOT to AA1, indexed aortic diameters correlated significantly with $WSS_{M,avg}$ ($R=-0.32$, $P<.01$), $WSS_{A,avg}$ ($R=-0.51$, $P<.01$). $WSS_{C,avg}$ and $WSS_{C,max}$ did not significantly correlate with indexed diameter.

3.5. Associations with aortic remodelling – multivariable analysis

A multiple linear regression model was constructed to assess for independent associations of age, EL_{index}, PD_{sys}, $WSS_{M,avg}$, $WSS_{A,avg}$, and $WSS_{C,avg}$ to indexed aortic dimensions inclusive of all aortic segments. The model had an overall *R* value of 0.60 and demonstrated $WSS_{M,avg}$ ($\beta=-0.36$, $P<.01$), $WSS_{A,avg}$ ($\beta=-0.26$, $P<.01$), and EL_{index} ($\beta=0.20$, $P=.01$) to be most significantly associated with indexed diameter in the ascending aorta.

4. Discussion

Our study investigated thoracic aortic hemodynamics and PD in BAV patients with comparison to healthy volunteers with tricuspid aortic valve morphology. Three main findings were identified:

(1) BAV patients have greater peak systolic PD and EL than controls throughout the AAo,
(2) BAV patients exhibit significantly greater $WSS_{C,avg}$ and localized maximum WSS-based measures than controls in the AAo, and
(3) AAo diameter associates with circumferentially averaged peak systolic WSS_M and WSS_A and EL_{index}.

4.1. Viscous energy loss and pressure drop in BAV patients versus controls

Significantly higher EL_{sys}, EL_{index}, and PD_{sys} were observed in the AAo of BAV patients compared to healthy controls. The measurement of these parameters in the context of BAV disease is novel, and therefore comparison to previous literature is very limited. This said, aortic EL and pressure loss are known to increase in the presence of valve stenosis, aortic dilation, and abnormal helical flow,[7,22,25,26] all of which typically accompany BAV aortopathy. Hence, the elevated EL and PD observed in our BAV disease population is consistent with prior knowledge.

Because EL represents a permanent loss of blood flow kinetic energy due to thermal dissipation, it is believed to be an important indicator of LV efficiency.[7] The greater aortic EL present, the greater the amount of work the LV must perform to compensate for these energy losses. Thus, increases in AAo EL observed in BAV disease may contribute to abnormal LV workload, LV remodelling, and related adverse cardiovascular outcomes.

Pressure gradients are conventionally measured via invasive catheterization or TTE (transthoracic echocardiogram) and are used to estimate severity of valvular disease. However, they only represent local measurements and are known to overestimate irreversible pressure loss as they neglect downstream pressure recovery.[11,12] As a result, currently available pressure gradient measurements may be sub-optimal for assessing the severity of valve pathology and predicting clinical outcomes. Alternatively, PDs measured via MRI represent pressure changes along an entire volume of interest and can account for downstream pressure recovery.[13] For this reason, MRI-derived pressure drop measurements may provide more accurate pressure mapping of the aorta and clinical utility in the evaluation of BAV disease severity. The PD findings presented in this study are novel and contribute to the development of clinically feasible methods of pressure gradient derivation.

4.2. WSS measures in BAV versus controls

In comparison to healthy controls, BAV patients showed several WSS-based differences. Most prominently, BAV patients exhibited significantly greater $WSS_{C,avg}$ throughout the entire AAo. The increase in $WSS_{C,avg}$ within this population agrees with previous literature and is believed to be a result of increased flow helicity/eccentricity generated by post-valvular flow displacement.[27,28] However, the BAV cohort demonstrated slightly lower $WSS_{M,avg}$ compared to the control cohort (statistically significant at LVOT and SOV regions only), which was unexpected as previous studies evaluating age- and size-matched BAV and control cohorts have reported higher $WSS_{M,avg}$ in BAV cohorts.[27,29,30] The observed discrepancy of our findings for $WSS_{M,avg}$ may reflect limitations in its derivation. WSS values calculated via the methods used in this study are dependent on spatial resolution and segmentation quality.[31,32] For example, Potters et al found that segmentation errors could result in systematic WSS quantification inaccuracies of up to 40%. Due to significant differences in AAo size between our control and patient cohorts, it is possible the quality of AAo segmentations also differed between each cohort, creating discrepancies in the analyses of WSS values at the fluid–wall interface.

In contrast to circumference-averaged WSS findings, each of the localized maximum WSS values – $WSS_{M,max}$, $WSS_{A,max}$, and $WSS_{C,max}$ – were significantly greater in BAV patients at the MAA level. Similarly, matched no dilated BAV and controls subcohort identified these trends. It is possible these differences are significant only at the MAA because this is where the most drastic hemodynamic alterations occur in those with valve disease and the sensitivity of localized maximum WSS measurements may succumb to noise effects at other aortic locations.

4.3. Associations of 4D flow-based measures and aortic diameter

Throughout the AAo, $WSS_{M,avg}$ and $WSS_{A,avg}$ was reduced in patients with dilated aortas and was inversely associated with aortic diameters via univariate and multivariate analyses. Previous studies support this inverse relationship between WSS_M and vessel diameter[30,33] and have documented that elevated WSS may be a catalyst for remodeling pathways within the aorta.[14,34,35] It is therefore important to recognize that WSS may exhibit an intimate and dynamic relationship with aortic vessel diameter; however, expanded work with longitudinal studies capable of delineating this dynamic interaction are required. Future studies aimed at exploring this interaction may want to utilize circumference-averaged WSS measurements, as this study suggests that circumference-averaged WSS shares a greater association with aortic dilation than localized maximum WSS.

Finally, we observed a positive association between EL_{index} and indexed aortic diameter in our study. Similar findings have been previously observed in BAV patients and interpreted as the result of induced helical flow due to vessel dilation.[22] While normal aortic diameters maintain fairly streamline flow patterns, vessel dilation inherently promotes helical flow and vortical formations. Blood particles traveling through the aorta along a helical trajectory must experience a longer travel distance and, therefore, will experience larger kinetic energy losses. Our observed associations between EL_{index} and indexed diameter is therefore may be reflective of this phenomenon; however, it is important to note that our study design does not allow for any causational links to be drawn from the results.

4.4. Study limitations

This study has several limitations. First, our cohort sizes were modest, particularly for control and type 0 valve cohorts, which hinders the generalizability of our findings. Second, BAV patients were only included if they underwent clinically ordered MRI examinations. At our centre this is typically for the evaluation of aortic dilation or significant valvular stenosis and/or insufficiency. Accordingly, our study cohort had a more severe disease phenotype than prior studies. Third, as a cross-sectional design, no causative relationships can be determined from our analyses.

In addition, WSS values were not regionally defined according to sub-segmental distribution (i.e., according to radially oriented sub-regions). Such analyses were not feasible using the available software but may provide more comprehensive insights regarding aortic flow patterns of BAV disease in general or BAV sub-types specifically. Finally, we obtained only peak systolic measurements of advanced flow parameters, as opposed to measuring values that are time-averaged over the cardiac cycle. This allows us to focus on the cardiac cycle phase in which valvular disease likely has the greatest impact (i.e., systole); however, it renders our data more sensitive to noise.

Technical limitations are also present in this study. First, the temporal and spatial resolution of MRI is adequate, yet, relatively low compared to other imaging modalities. Second, our calculation of WSS, PD, and EL values involves partial derivatives and interpolation. Combined with the limited temporal and spatial resolution, this creates marginal underestimations in the calculation of WSS, PD, and EL.[32] However, such underestimations should not impact our analyses, as our conclusions were based on relative differences between groups and associations between parameters.

In conclusion, a clinically referred BAV patient cohort we observed significant elevations in aortic WSS_C, EL, and PD relative to healthy controls. Peak systolic WSS_M and WSS_A demonstrate moderate associations with aortic diameter in the BAV population. This study highlights the potential utility of EL, PD, and WSS sub-vectors as biomarkers in BAV disease severity and aortic dilation assessment.

Author contributions

Conceptualization: Paul W.M. Fedak, James A. White, Julio Garcia.
Data curation: Patrick Geeraert, Fatemehsadat Jamalidinan, Michael Bristow, Carmen Lydell, Julio Garcia.
Formal analysis: Patrick Geeraert, Fatemehsadat Jamalidinan, Alireza Sojoudi, Michael Bristow, Carmen Lydell, Julio Garcia.
Funding acquisition: Patrick Geeraert, James A. White, Julio Garcia.
Investigation: Patrick Geeraert, Fatemehsadat Jamalidinan, Alireza Sojoudi, Michael Bristow, Carmen Lydell, Paul W.M. Fedak, James A. White, Julio Garcia.
Methodology: Ali Fatehi Hassanabad, Alireza Sojoudi, Paul W. M. Fedak, James A. White, Julio Garcia.
Project administration: Julio Garcia.
Resources: Paul W.M. Fedak, Julio Garcia.

Software: Fatemehsadat Jamalidinan, Alireza Sojoudi, Julio Garcia.
Supervision: Fatemehsadat Jamalidinan, Ali Fatehi Hassanabad, James A. White, Julio Garcia.
Validation: Ali Fatehi Hassanabad.
Visualization: Fatemehsadat Jamalidinan, Julio Garcia.
Writing – original draft: Patrick Geeraert.
Writing – review & editing: Fatemehsadat Jamalidinan, Ali Fatehi Hassanabad, Alireza Sojoudi, Michael Bristow, Carmen Lydell, Paul W.M. Fedak, James A. White, Julio Garcia.

References

[1] Ward C. Clinical significance of the bicuspid aortic valve. Heart 2000;83:81–5.
[2] Michelena HI, Khanna AD, Mahoney D, et al. Incidence of aortic complications in patients with bicuspid aortic valves. JAMA 2011; 306:1104–12.
[3] Tzemos N, Therrien J, Yip J, et al. Outcomes in adults with bicuspid aortic valves. JAMA 2008;300:1317–25.
[4] Baumgartner H, Falk V, Bax JJ, et al. 2017 ESC/EACTS guidelines for the management of valvular heart disease. Eur Heart J 2017;38:2739–91.
[5] Borger MA, Fedak PWM, Stephens EH, et al. The American Association for Thoracic Surgery consensus guidelines on bicuspid aortic valve-related aortopathy: full online-only version. J Thorac Cardiovasc Surg 2018;156:e41–74. doi 10.1016/j.jtcvs.2018.02.115.
[6] Verma S, Yanagawa B, Kalra S, et al. Knowledge, attitudes, and practice patterns in surgical management of bicuspid aortopathy: a survey of 100 cardiac surgeons. J Thorac Cardiovasc Surg 2013;146:1033–40.
[7] Akins CW, Travis B, Yoganathan AP. Energy loss for evaluating heart valve performance. J Thorac Cardiovasc Surg 2008;136:820–33.
[8] Ebbers T, Farnebäck G. Improving computation of cardiovascular relative pressure fields from velocity MRI. J Magn Reson Imaging 2009;30:54–61.
[9] Hassanabad AF, Burns F, Bristow MS, et al. Pressure drop mapping using 4D flow MRI in patients with bicuspid aortic valve disease: a novel marker of valvular obstruction. Magn Reson Imaging 2020;65:175–82.
[10] Lamata P, Pitcher A, Krittian S, et al. Aortic relative pressure components derived from four-dimensional flow cardiovascular magnetic resonance. Magn Reson Med 2014;72:1162–9.
[11] Garcia D, Pibarot P, Dumesnil JG, Sakr F, Durand LG. Assessment of aortic valve stenosis severity. Circulation 2000;101:765–71.
[12] Pibarot P, Garcia D, Dumesnil JG. Energy loss index in aortic stenosis: from fluid mechanics concept to clinical application. Circulation 2013;127:1101–4.
[13] Garcia J, Capoulade R, Gaillard E, Kadem L, Pibarot P, Larose E. Discrepancies between cardiovascular magnetic resonance and doppler-echocardiography in the measurement of transvalvular gradient in aortic stenosis severity: the effect of flow vorticity. J Cardiovasc Magn Reson 2013;15:84.
[14] Guzzardi DG, Barker AJ, Van Ooij P, et al. Valve-related hemodynamics mediate human bicuspid aortopathy. J Am Coll Cardiol 2015;66:892–900.
[15] Stalder AF, Russe MF, Frydrychowicz A, Bock J, Hennig J, Markl M. Quantitative 2D and 3D phase contrast MRI: optimized analysis of blood flow and vessel wall parameters. Magn Reson Med 2008;60:1218–31.
[16] Markl M, Harloff A, Bley TA, et al. Time-resolved 3D MR velocity mapping at 3T: improved navigator-gated assessment of vascular anatomy and blood flow. J Magn Reson Imaging 2007;25:824–31.
[17] Garcia J, van der Palen RLF, Bollache E, et al. Distribution of blood flow velocity in the normal aorta: effect of age and gender. J Magn Reson Imaging 2018;47:487–98.
[18] Garcia J, Barker AJ, Collins JD, Carr JC, Markl M. Volumetric quantification of absolute local normalized helicity in patients with bicuspid aortic valve and aortic dilatation. Magn Reson Med 2017;78:689–701.
[19] Hiratzka LF, Bakris GL, Beckman JA, et al. 2010 ACCF/AHA/AATS/ACR/ASA/SCA/SCAI/SIR/STS/SVM guidelines for the diagnosis and management of patients with thoracic aortic disease. J Am Coll Cardiol 2010;55:e27–129.
[20] Caruthers SD, Lin SJ, Brown P, et al. Practical value of cardiac magnetic resonance imaging for clinical quantification of aortic valve stenosis: comparison with echocardiography. Circulation 2003;108:2236–43.
[21] Cawley PJ, Maki JH, Otto CM. Cardiovascular magnetic resonance imaging for valvular heart disease: technique and validation. Circulation 2009;119:468–78.
[22] Barker AJ, van Ooij P, Bandi K, et al. Viscous energy loss in the presence of abnormal aortic flow. Magn Reson Med 2014;72:620–8.
[23] Davies RR, Gallo A, Coady MA, et al. Novel measurement of relative aortic size predicts rupture of thoracic aortic aneurysms. Ann Thorac Surg 2006;81:169–77.
[24] Sievers H-H, Schmidtke C. A classification system for the bicuspid aortic valve from 304 surgical specimens. J Thorac Cardiovasc Surg 2007;133:1226–33.
[25] Garcia J, Capoulade R, Le Ven F, et al. Discrepancies between cardiovascular magnetic resonance and Doppler echocardiography in the measurement of transvalvular gradient in aortic stenosis: the effect of flow vorticity. J Cardiovasc Magn Reson 2013;15:84. doi: 10.1186/1532-429X-15-84.
[26] Ha H, Kvitting JP, Dyverfeldt P, Ebbers T. 4D Flow MRI quantification of blood flow patterns, turbulence and pressure drop in normal and stenotic prosthetic heart valves. Magn Reson Imaging 2019;55: 118–27.
[27] Bissell MM, Hess AT, Biasiolli L, et al. Aortic dilation in bicuspid aortic valve disease: flow pattern is a major contributor and differs with valve fusion type. Circ Cardiovasc Imaging 2013;6:499–507.
[28] Rodríguez-Palomares JF, Dux-Santoy L, Guala A, et al. Aortic flow patterns and wall shear stress maps by 4D-flow cardiovascular magnetic resonance in the assessment of aortic dilatation in bicuspid aortic valve disease. J Cardiovasc Magn Reson 2018;20:28. doi: 10.1186/s12968-018-0451-1.
[29] Barker AJ, Markl M, Bürk J, et al. Bicuspid aortic valve is associated with altered wall shear stress in the ascending aorta. Circ Cardiovasc Imaging 2012;5:457–66.
[30] Farag ES, van Ooij P, Planken RN, et al. Aortic valve stenosis and aortic diameters determine the extent of increased wall shear stress in bicuspid aortic valve disease. J Magn Reson Imaging 2018;48:522–30.
[31] Potters WV, van Ooij P, Marquering H, VanBavel E, Nederveen AJ. Volumetric arterial wall shear stress calculation based on cine phase contrast MRI. J Magn Reson Imaging 2015;41:505–16.
[32] Cibis M, Potters WV, Gijsen FJ, et al. The effect of spatial and temporal resolution of cine phase contrast MRI on wall shear stress and oscillatory shear index assessment. PLoS One 2016;11:e0163316. doi: 10.1371/journal.pone.0163316.
[33] Truong U, Fonseca B, Dunning J, et al. Wall shear stress measured by phase contrast cardiovascular magnetic resonance in children and adolescents with pulmonary arterial hypertension. J Cardiovasc Magn Reson 2013;15:81. doi: 10.1186/1532-429X-15-81.
[34] Bollache E, Guzzardi DG, Sattari S, et al. Aortic valve-mediated wall shear stress is heterogeneous and predicts regional aortic elastic fiber thinning in bicuspid aortic valve-associated aortopathy. J Thorac Cardiovasc Surg 2018;156:2112–20e2.
[35] Tadros TM, Klein MD, Shapira OM. Ascending aortic dilatation associated with bicuspid aortic valve: pathophysiology, molecular biology, and clinical implications. Circulation 2009;119:880–90.